Evidence for the formation of SiGe nanoparticles in Ge-implanted Si_3N_4

S. Mirzaei, F. Kremer, R. Feng, C. J. Glover, and D. J. Sprouster

Citation: Journal of Applied Physics **121**, 105702 (2017); doi: 10.1063/1.4977507
View online: http://dx.doi.org/10.1063/1.4977507
View Table of Contents: http://aip.scitation.org/toc/jap/121/10
Published by the American Institute of Physics

Articles you may be interested in

A room-temperature-operated Si LED with β-$FeSi_2$ nanocrystals in the active layer: μW emission power at 1.5 μm
Journal of Applied Physics **121**, 113101 (2017); 10.1063/1.4978372

Resonant optical properties of AlGaAs/GaAs multiple-quantum-well based Bragg structure at the second quantum state
Journal of Applied Physics **121**, 103101 (2017); 10.1063/1.4978252

Mechanical and electronic properties of SiC nanowires: An ab initio study
121, 104302104302 (2017); 10.1063/1.4977996

Investigating the origins of high multilevel resistive switching in forming free Ti/TiO_{2-x}-based memory devices through experiments and simulations
Journal of Applied Physics **121**, 094501 (2017); 10.1063/1.4977063

Molecular beam epitaxy of 2D-layered gallium selenide on GaN substrates
Journal of Applied Physics **121**, 094302 (2017); 10.1063/1.4977697

Morphology of ion irradiation induced nano-porous structures in Ge and $Si_{1-x}Ge_x$ alloys
Journal of Applied Physics **121**, 115705 (2017); 10.1063/1.4978592

JOURNAL OF APPLIED PHYSICS **121**, 105702 (2017)

Evidence for the formation of SiGe nanoparticles in Ge-implanted Si_3N_4

S. Mirzaei,[1,a)] F. Kremer,[1] R. Feng,[1] C. J. Glover,[2] and D. J. Sprouster[3]
[1]*Department of Electronic Materials Engineering, Australian National University, Canberra, Australian Capital Territory 0200, Australia*
[2]*Australian Synchrotron, 800 Blackburn Road, Clayton, Australia*
[3]*Nuclear Science and Technology Department, Brookhaven National Laboratory, Upton, New York 11973, USA*

(Received 16 December 2016; accepted 14 February 2017; published online 14 March 2017)

SiGe nanoparticles were formed in an amorphous Si_3N_4 matrix by Ge^+ ion implantation and thermal annealing. The size of the nanoparticles was determined by transmission electron microscopy and their atomic structure by x-ray absorption spectroscopy. Nanoparticles were observed for excess Ge concentrations in the range from 9 to 12 at. % after annealing at temperatures in the range from 700 to 900 °C. The average nanoparticle size increased with excess Ge concentration and annealing temperature and varied from an average diameter of 1.8 ± 0.2 nm for the lowest concentration and annealing temperature to 3.2 ± 0.5 nm for the highest concentration and annealing temperature. Our study demonstrates that the structural properties of embedded SiGe nanoparticles in amorphous Si_3N_4 are sensitive to the implantation and post implantation conditions. Furthermore, we demonstrate that ion implantation is a novel pathway to fabricate and control the SiGe nanoparticle structure and potentially useful for future optoelectronic device applications. *Published by AIP Publishing.*
[http://dx.doi.org/10.1063/1.4977507]

INTRODUCTION

Semiconductor nanoparticles (NPs) are novel material systems with unique properties, which can be controlled by their size, structure, and host matrix.[1–5] Their exceptional optical and electrical properties make them ideal for optoelectronic and non-volatile memory devices.[6–8] The luminescence and nonlinear optical properties of Si and Ge NPs embedded in an SiO_2 matrix, and to a lesser extent in Si_3N_4, have been previously reported in Refs. 9–16. The structure and electrical properties of SiGe NPs are intrinsically linked to the size, shape, surface condition, atomic composition, and compositional uniformity.[9,17–19] A better understanding of the role of the matrix in the properties of NPs could lead to the fabrication of more efficient optoelectronic devices. In this study, ion implantation was used to produce $Si_{1-x}Ge_x$ NPs in an amorphous Si_3N_4 layer, which has a higher dielectric constant than SiO_2, and could prove to be a pathway for more efficient optoelectronic devices.

Here, we focus on the structural properties of SiGe NPs formed in low pressure chemical vapour deposition (LPCVD) Si_3N_4 layers as a function of Ge concentration and annealing temperature. A combination of complementary techniques including transmission electron microscopy (TEM) and synchrotron-based methods of X-ray-absorption Near-Edge Structure (XANES) and Extended X-ray-absorption Fine-Structure spectroscopy (EXAFS) has been utilized to characterize the size and structure of the embedded NPs. By combining results from these techniques, we achieved a detailed understanding of the bonding environment and structural properties of the NPs as a function of implantation and post-implantation annealing conditions.

a)sahar.mirzaei@anu.edu.au

EXPERIMENTAL PROCEDURE

$^{74}Ge^{+1}$ ions were implanted into 2 μm amorphous LPCVD Si_3N_4 layers grown on Si (100) wafers with an energy of 1.3 MeV to fluences of either 3.6 or 4.8×10^{17} ions/cm^{-2}. To promote NP nucleation and growth, the substrate was maintained at 400 °C during implantation. Samples were then annealed post implantation for 1 h in a N_2 ambient at 700 or 900 °C.

Cross-section TEM images were obtained in the bright field mode using a JEOL 2100F microscope operating at 200 kV. Samples were prepared with a standard mechanical polishing and ion-beam-milling protocols.

XANES and EXAFS measurements were performed at the Ge *K*-edge (11.103 keV) at a temperature of 15 K at the XAS beamline of the Australian Synchrotron. Fluorescence-mode spectra were recorded with a 10×10 Ge pixel-array detector. Data were collected to a photoelectron wavenumber (k) of 13.5 $Å^{-1}$. To predict energy drifting, a crystalline Ge (c-Ge) reference foil was simultaneously measured in the transmission mode. Bulk crystalline and amorphous $Si_{1-x}Ge_x$ alloys previously characterized[19] were also measured to compare against the NP samples. The Si substrate below the Ge-implanted Si_3N_4 layer was removed by mechanical grinding and selective chemical etching with KOH to improve the signal-to-noise ratio for the XAS measurements and remove unwanted scatter from the substrate. The Ge-implanted layers were stacked together and then mounted on the sample holder with kapton tape.[20] The amorphous Ge (a-Ge) sample was prepared by ion implantation described elsewhere.[21]

The absorption spectra were first averaged with the program AVERAGE.[22] The averaged data were then processed and analysed by ATHENA and ARTEMIS.[23] EXAFS spectra

were Fourier-transformed FT over a k-range of 3.7–12.0 $\mathrm{\AA}^{-1}$ and back FT over a non-phase corrected radial distance (R-range) of 1.3–2.7 Å to isolate the scattering contribution from the first-nearest-neighbour (FNN). Effective scattering amplitudes and phase shifts were calculated *ab initio* with FEFF8. To minimize the number of refined variables, S_0^2 and ΔE_0 were deduced from the crystalline Ge sample and held constant thereafter for the analysis of the NP samples. For bulk c-Ge, the value of the amplitude reduction factor (S_0^2) and threshold energy (ΔE_0) was determined to be 0.94 ± 0.1 and 3.7 ± 0.9 eV, respectively. The structural properties of the NP samples were determined using a FEFF-generated Ge_xSi_{1-x} random structure. The coordination number ($CN_{Ge\text{-}Ge}$) was fixed to four for the bulk c-Ge and allowed to refine for the NP samples including CNs for the separate Ge ($CN_{Ge\text{-}Ge}$) and Si ($CN_{Ge\text{-}Si}$) components. The Ge and Si bondlengths ($R_{Ge\text{-}Ge}$ and $R_{Ge\text{-}Si}$) and Debye-Waller factors ($\sigma^2_{Ge\text{-}Ge}$, $\sigma^2_{Ge\text{-}Si}$) were allowed to vary during the fitting. The Debye-Waller factors for the Ge-Ge and Ge-Si bonds ($\sigma^2_{Ge\text{-}Ge}$ and $\sigma^2_{Ge\text{-}Si}$, respectively) were restrained such that $\sigma^2_{Ge\text{-}Ge} = \sigma^2_{Ge\text{-}Si}$, consistent with previous theoretical and experimental reports.[19] The structural parameters determined using our method included here included CN_{Ge}, CN_{Si}, $R_{Ge\text{-}Ge}$, $R_{Ge\text{-}Si}$, and $\sigma^2_{Ge\text{-}Ge}$, with $\sigma^2_{Ge\text{-}Ge} = \sigma^2_{Ge\text{-}Si}$.

RESULTS AND DISCUSSION

Figure 1 shows representative TEM images of the $Si_{1-x}Ge_x$ NPs. These correspond to samples implanted to a peak Ge concentration of 9, Fig. 1(a), and 12 at. %, Fig. 1(c), after annealing at 700 and 900 °C, respectively. NP size distributions were determined from TEM by measuring the diameters of 100 representative particles, as shown in Figs. 1(b) and 1(d). The average NP diameters for each sample are summarized in Table I. The average NP diameter clearly increases as the implanted Ge concentration or annealing temperature increase. High-resolution TEM images of individual NPs are included in the insets of Figs. 1(b) and 1(d). These highlight the difficulty of extracting structural information from such a small NP. Indeed, the lack of clearly defined crystal planes and the small volume fraction of materials available for diffraction analysis make it impractical to distinguish between Ge and $Si_{1-x}Ge_x$ NP, particularly given the small lattice mismatch between Ge and $Si_{1-x}Ge_x$, which is expected to be ≤1%. The small increase in NP size is due to the low diffusivity of Ge atoms in Si_3N_4. The depth distribution of Ge atoms before and after thermal annealing demonstrates that the post implantation thermal annealing did not lead to a significant loss or redistribution of Ge atoms. This is potentially due to the rigid structure of LPCVD Si_3N_4 layers[24] and low mobility of Ge in Si_3N_4.[15]

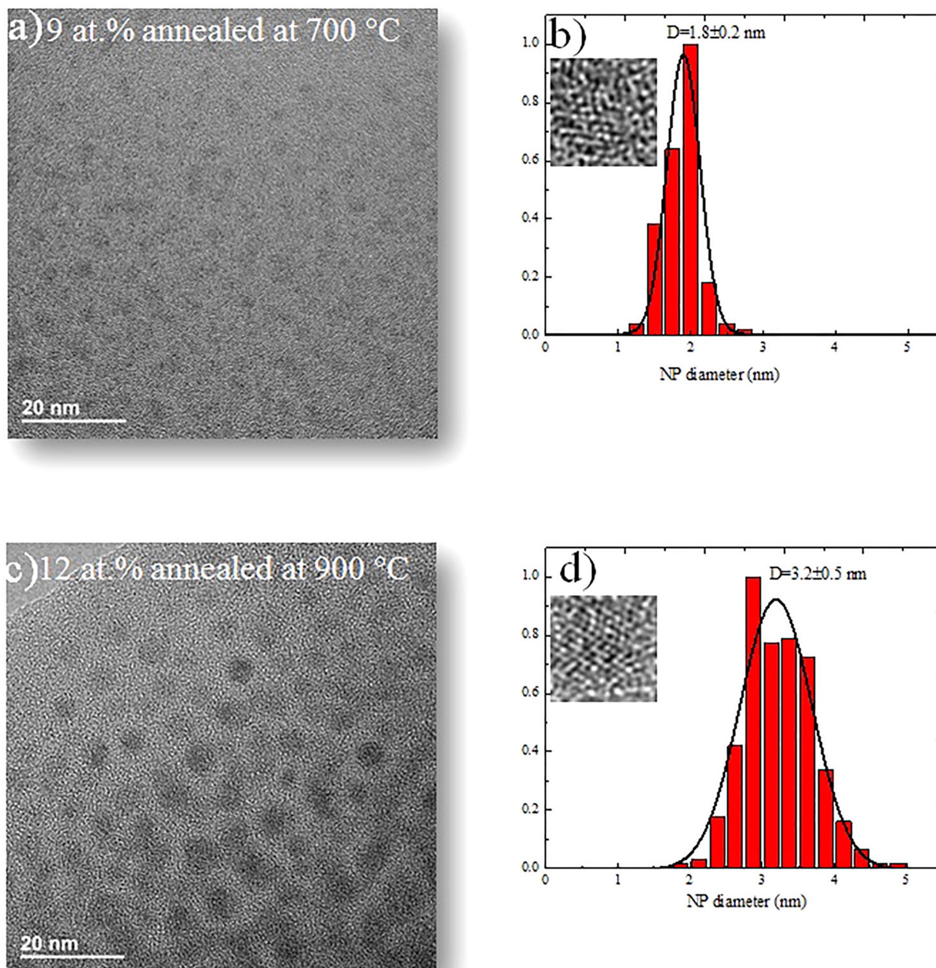

FIG. 1. TEM images of 9 and 12 at.% NPs after annealing at 700 and 900 °C, respectively. The determined size distributions are plotted adjacent.

TABLE I. Structural parameters—interatomic distance R, Debye-Waller factors σ^2, and coordination numbers CN—obtained for the FNN of NPs. Total CN increases with an increase in temperature.

	Annealing temperature (°C)	NP size (nm)	CN-Ge (atoms)	R-Ge (Å)	CN-Si (atoms)	R-Si (Å)	DW (10^{-3} Å^2)
9 at.%	700	1.8 ± 0.2	0.9 ± 0.1	2.446 ± 0.008	1.6 ± 0.2	2.382 ± 0.001	3.3 ± 0.3
	900	2.2 ± 0.3	1.3 ± 0.2	2.445 ± 0.007	1.7 ± 0.2	2.391 ± 0.003	3.2 ± 0.2
12 at. %	700	2.8 ± 0.5	1.6 ± 0.1	2.447 ± 0.004	1.4 ± 0.1	2.387 ± 0.008	3.5 ± 0.4
	900	3.2 ± 0.5	2.5 ± 0.1	2.451 ± 0.005	1.2 ± 0.1	2.389 ± 0.004	3.2 ± 0.5
c-$Si_{80}Ge_{20}$ [a]				2.428		2.383	1.9 ± 0.3
a-$Si_{80}Ge_{20}$ [a]				2.438		2.399	3.5 ± 0.6
c-$Si_{57}Ge_{43}$ [a]				2.429		2.381	1.9 ± 0.3
a-$Si_{57}Ge_{43}$ [a]				2.447		2.400	3.5 ± 0.6
c-$Si_{22}Ge_{78}$ [a]				2.441		2.388	1.9 ± 0.3
a-$Si_{22}Ge_{78}$ [a]				2.452		2.396	3.5 ± 0.6
$Si_{38}Ge_{62}$ [b]		16 ± 2		2.441 ± 0.001		2.370	2.3

[a]Ref. 19 crystalline and amorphous standards.
[b]Ref. 31 SiGe NPs embedded in the SiO_2 matrix (the total coordination number is fixed to 3.77).

The chemical bonding of the NPs was initially determined with XANES, and representative spectra for the 9 and 12 at. % Ge samples are shown in Figure 2 as a function of annealing temperature. The crystalline and amorphous Ge and $Si_{1-x}Ge_x$ standards are included for reference (adopted from Ref. 19). The specific features observed in the XANES are the result of multiple scattering resonances, particular to the crystallographic phase and chemical environment of the absorbing Ge atoms. For the samples annealed at 700 °C, there is a lack of appreciable structure, and spectra are similar in shape to the amorphous standards. Figure 2 shows features in the NP spectra at ∼11 123 and ∼11 130 eV that are also more like the c-SiGe spectra (and absent in the a-Ge standard). Samples annealed at 900 °C show additional changes in the XANES including an increase in the intensity at ∼11 106 eV and the formation of a small valley at ∼11 108 eV similar to the c-SiGe standards.

The changes in the near-edge structure (relative to the bulk structure) potentially indicate that the NP structure changes with annealing temperature. The XANES spectra of NP samples shown in Figure 2 resemble the SiGe standards

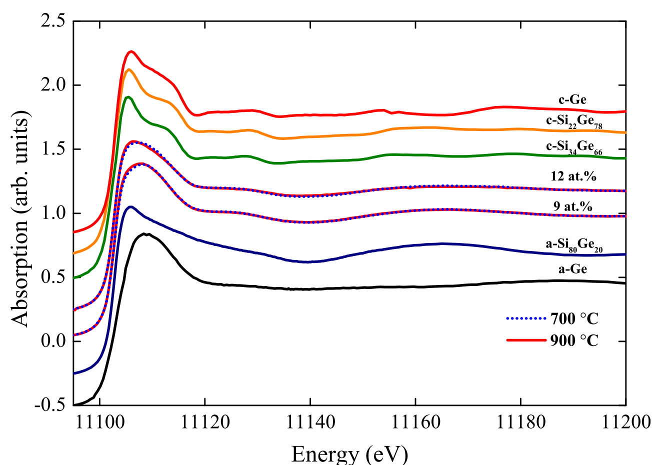

FIG. 2. XANES spectra of 9 and 12 at. % after annealing at 700 or 900 °C samples plus crystalline and amorphous Ge and $Si_{22}Ge_{78}$, $Si_{66}Ge_{34}$, and amorphous $Si_{80}Ge_{20}$ standards. The spectra have been offset for clarity.

more than the Ge standards. Furthermore, the NP spectra show evidence of a combination of amorphous and crystalline environments. This combination of crystalline and amorphous environments is consistent with previous studies[25,26] where the formation of an amorphous surface layer separating the crystalline NP core was observed in embedded Ge NPs. Finally, no evidence of Ge nitride formation was apparent from the XANES analysis.[27,28] The preferential Ge-Si bonding is potentially attributed to the lower bonding energy of Si and Ge (∼297 kJ/mol)[29] and a larger number of free Si bonds in the nitride matrix.

Figures 3(a), 3(c), and 3(e) show the isolated k^3-weighted EXAFS oscillations, and Figures 3(b), 3(d), and 3(f) show the corresponding FT spectra for the standards and NP samples annealed at 700 or 900 °C. The peaks in the FT EXAFS spectra for the crystalline standards are the result of scattering from single and multiple scattering atomic paths surrounding the Ge atoms in the diamond cubic crystal phase. Scattering contributions from the first, second, and third nearest neighbour shells are apparent in the c-Ge and c-$Si_{1-x}Ge_x$ standards (adopted from Ref. 19), consistent with a diamond cubic structure. In the a-$Si_{80}Ge_{20}$ sample, Ge-Ge and Ge-Si shells in the FNN are observed with no fine features apparent after the ∼2Å peak. The amplitudes of the peaks in the NP samples are significantly reduced compared to the bulk counterparts and increase slightly with annealing temperature (or particle size). This is commonly observed in NP samples, where both a decrease in the average coordination and an increase in structural disorder yield reductions in the EXAFS peak amplitudes.[26] Interestingly, the fine structure in the NP samples' second and third nearest neighbour peaks is significantly lower in amplitude compared to the bulk samples, indicating that the NPs are heavily disordered. This result is consistent with previous reports of Ge NPs that show a similar decrease in higher neighbour.[26]

The refined fitting parameters for the NP FNN shells are listed in Table I. The results from previous studies[19,30,31] are also listed in Table I for reference. The changes in the structural parameters are consistent with the qualitative description described above, with the formation of a combination of

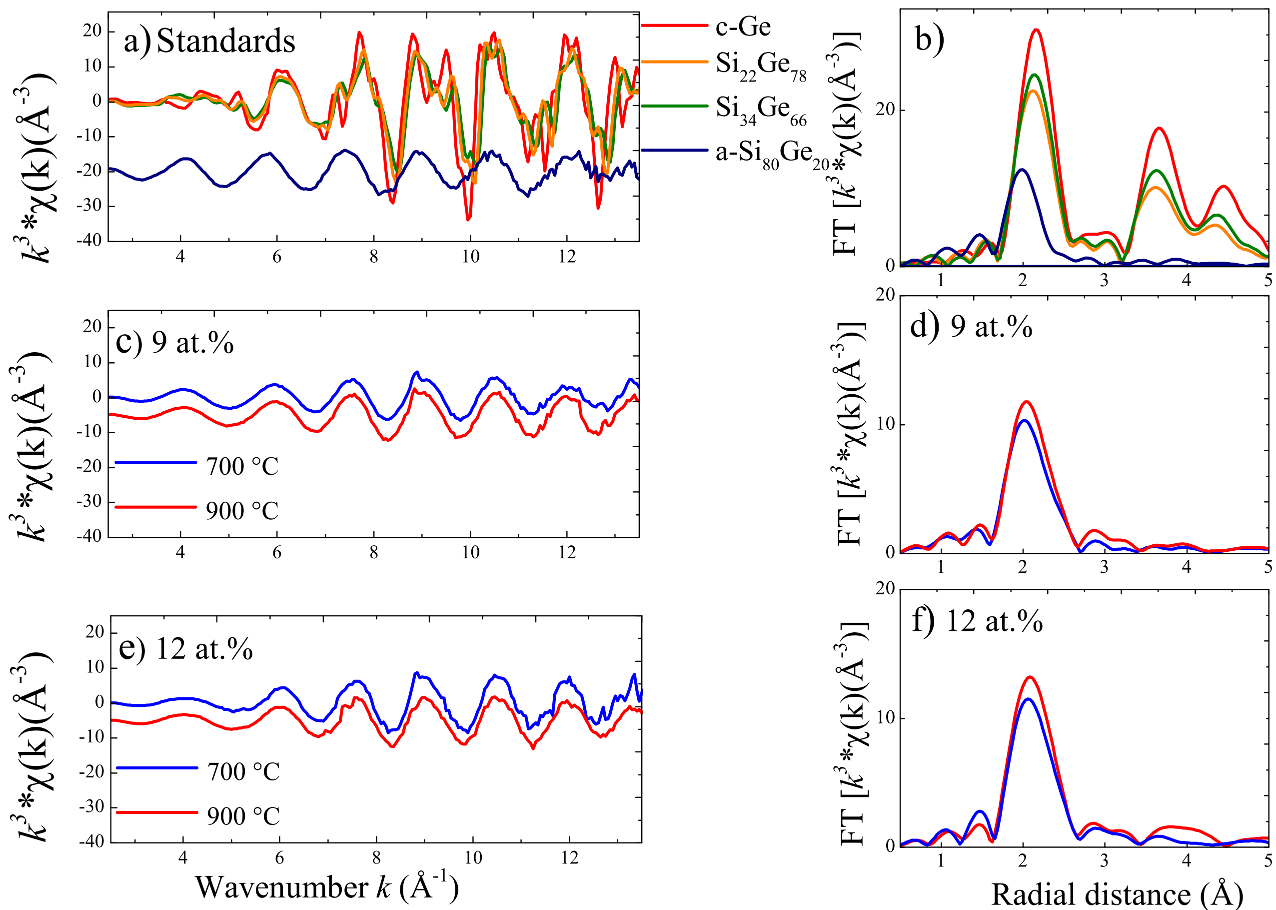

FIG. 3. EXAFS spectra ((a), (c), and (e)) and FT EXAFS ((b), (d), and (f)) for bulk standards, 9 at. % and 12 at. % NP samples. The spectra in ((a), (c), and (e)) have been offset for clarity. The first NN in the FT spectra is interpreted as Ge-Ge and Ge-Si shell.

amorphous and crystalline phases. The $R_{Ge\text{-}Si}$ and $R_{Ge\text{-}Ge}$ of the NPs are slightly higher than their bulk crystalline counterparts (included in Table I) and increase slightly with increasing annealing temperature (or increase in NP size). The larger $R_{Ge\text{-}Si}$ and $R_{Ge\text{-}Ge}$ measured here are directly attributed to the non-negligible fraction of surface amorphous/disordered atoms that dominate at the low annealing temperature or concomitantly small NP size. The Debye-Waller factor for the NPs is significantly larger compared to crystalline standards and similar in value to those determined for the amorphous standards. The large Debye-Waller factors thus indicate that the structure is predominately disordered, for these formation conditions. The decrease in the $CN_{Ge\text{-}Si}$ and increase in the $CN_{Ge\text{-}Ge}$ after the 900 °C annealing, with only a small change in NP size, potentially indicate that the composition of the NPs changes with increasing annealing temperature. Additionally, the EXAFS (and XANES) results for the 12 at.% samples show that the combination of high-concentration and high-annealing temperature induces an increase in the fraction of atoms in a crystalline environment.

CONCLUSION

Here, we have shown that the combination of ion implantation and thermal annealing of Ge ions into LPCVD a-Si_3N_4 films results in $Si_{1-x}Ge_x$ NPs with a dominant disordered crystal structure, as evidenced by XANES and EXAFS measurements. The concentration- and annealing temperature-dependent trends in the atomic structure also show that the coordination environment/composition of the NPs changes subtly with annealing temperature, resulting in Ge-rich NPs. The preferential Ge-Si bonding quantified here is attributed to the lower bonding energy and larger number of free Si bonds in the nitride matrix. The small NP size and slow precipitate growth with relatively high Ge concentrations and annealing temperatures are the direct result of a low Ge mobility in Si_3N_4. This highlights the role of the matrix in the embedded nanostructure properties. Thin films containing $Si_{1-x}Ge_x$ NPs are important for future applications in optoelectronic devices because of their band gap tunability. Furthermore, the ability to control the structure (crystalline/disordered), size, and chemical composition of the SiGe NPs highlights the flexibility of our simple approach with potential applications in future optical devices.

ACKNOWLEDGMENTS

We dedicate this publication to Professor Mark Ridgway (deceased), who loved physics and was a significant driver of this research. SM acknowledges his excellent supervision, enthusiasm and encouragement, especially his instruction at the Australian Synchrotron on

and X-Ray Absorption Spectroscopy (XAS) beamline. We acknowledge access to NCRIS infrastructure at the Australian National University including the Australian National Fabrication Facility and the Heavy Ion Accelerator Capability. We also thank the Australian Research Council and Australian Synchrotron for support. Access to the facilities of the Centre for Advanced Microscopy, with funding through the Australian Microscopy and Microanalysis Research Facility, is gratefully acknowledged.

[1]X. Zhong, Y. Feng, I. Lieberwirth, and W. Knoll, Chem. Mater. **18**, 2468 (2006).
[2]E. Roduner, Chem. Soc. Rev. **35**, 583 (2006).
[3]J. Kennedy, J. Leveneur, Y. Takeda, G. Williams, S. Kupke, D. Mitchell, A. Markwitz, and J. Metson, J. Mater. Sci. **47**, 1127 (2012).
[4]J. Kennedy, J. Leveneur, G. Williams, D. Mitchell, and A. Markwitz, Nanotechnology **22**, 115602 (2011).
[5]J. Leveneur, G. I. Waterhouse, J. Kennedy, J. B. Metson, and D. R. Mitchell, J. Phys. Chem. C **115**, 20978 (2011).
[6]S. Takeoka, K. Toshikiyo, M. Fujii, S. Hayashi, and K. Yamamoto, Phys. Rev. B **61**, 15988 (2000).
[7]S. Ray and K. Das, Opt. Mater. **27**, 948 (2005).
[8]S. Ray, S. Maikap, W. Banerjee, and S. Das, J. Phys. D: Appl. Phys. **46**, 153001 (2013).
[9]J. G. Zhu, C. White, J. Budai, S. Withrow, and Y. Chen, J. Appl. Phys. **78**, 4386 (1995).
[10]V. Cantelli, J. Von Borany, A. Mücklich, and N. Schell, Nucl. Instrum. Methods Phys. Res., Sect. B **238**, 268 (2005).
[11]J. S. Jensen, T. L. Pedersen, R. Pereira, J. Chevallier, J. L. Hansen, B. B. Nielsen, and A. N. Larsen, Appl. Phys. A: Mater. Sci. Process. **83**, 41 (2006).
[12]A. Wellner, V. Paillard, C. Bonafos, H. Coffin, A. Claverie, B. Schmidt, and K. Heinig, J. Appl. Phys. **94**, 5639 (2003).
[13]A. Williamson, C. Bostedt, T. Van Buuren, T. Willey, L. Terminello, G. Galli, and L. Pizzagalli, Nano Lett. **4**, 1041 (2004).
[14]M. Derivaz, P. Noé, D. Jalabert, J. Rouviére, D. Buttard, D. Sotta, and A. Barski, Microelectron. Eng. **61**, 643 (2002).
[15]S. Mirabella, S. Cosentino, A. Gentile, G. Nicotra, N. Piluso, L. Mercaldo, F. Simone, C. Spinella, and A. Terrasi, Appl. Phys. Lett. **101**, 011911 (2012).
[16]A. M. Asaduzzaman and M. Springborg, Phys. Rev. B **74**, 165406 (2006).
[17]J. Tarus, M. Tantarimäki, and K. Nordlund, Nucl. Instrum. Methods Phys. Res., Sect. B **228**, 51 (2005).
[18]Y.-H. Kuo, Y. K. Lee, Y. Ge, S. Ren, J. E. Roth, T. I. Kamins, D. A. Miller, and J. S. Harris, Nature **437**, 1334 (2005).
[19]M. C. Ridgway, K. Yu, C. Glover, G. J. Foran, C. Clerc, J. L. Hansen, and A. N. Larsen, Phys. Rev. B **60**, 10831 (1999).
[20]S. Decoster, C. Glover, B. Johannessen, R. Giulian, D. J. Sprouster, P. Kluth, L. L. Araújo, Z. S. Hussain, C. Schnohr, and H. Salama, J. Synchrotron Radiat. **20**, 426 (2013).
[21]M. C. Ridgway, G. D. Azevedo, R. G. Elliman, C. J. Glover, D. J. Llewellyn, R. Miller, W. Wesch, G. J. Foran, J. Hansen, and A. Nylandsted-Larsen, Phys. Rev. B **71**, 094107 (2005).
[22]See http://www.synchrotron.org.au/aussyncbeamlines/x-ray-absorption-spectroscopy/data-analysis for information on how to convert the raw data from binary format into ascii and analyse them.
[23]B. Ravel and M. Newville, J. Synchrotron Radiat. **12**, 537 (2005).
[24]B. E. Deal and C. R. Helms, *The Physics and Chemistry of SiO2 and the Si-SiO2 Interface* (Springer, New York, USA, 1993), p. 187.
[25]S. Mirzaei, F. Kremer, D. Sprouster, L. Araujo, R. Feng, C. Glover, and M. C. Ridgway, J. Appl. Phys. **118**, 154309 (2015).
[26]L. Araujo, R. Giulian, D. Sprouster, C. Schnohr, D. Llewellyn, P. Kluth, D. Cookson, G. Foran, and M. Ridgway, Phys. Rev. B **78**, 094112 (2008).
[27]C. L. Bull, P. F. McMillan, J. P. Itié, and A. Polian, Phys. Status Solidi A **201**, 909 (2004).
[28]M. Micoulaut, L. Cormier, and G. Henderson, J. Phys.: Condens. Matter **18**, R753 (2006).
[29]Y.-R. Luo, *Comprehensive Handbook of Chemical Bond Energies* (CRC Press, Boca Raton, 2012).
[30]J. Aubry, T. Tyliszczak, A. Hitchcock, J.-M. Baribeau, and T. Jackman, Phys. Rev. B **59**, 12872 (1999).
[31]A. Gasperini, A. Malachias, G. Fabbris, G. Kellermann, A. Gobbi, E. Avendano, and G. d. M. Azevedo, J. Appl. Crystallogr. **45**, 71 (2012).